RSC Advances

ROYAL SOCIETY OF CHEMISTRY

www.rsc.org/advances

Table of Content

- Novel synthesis of C, N doped rice grain shaped visible active ZnS nano photocatalysts
- Enhanced activity for the pollutant removal and H_2 production from water

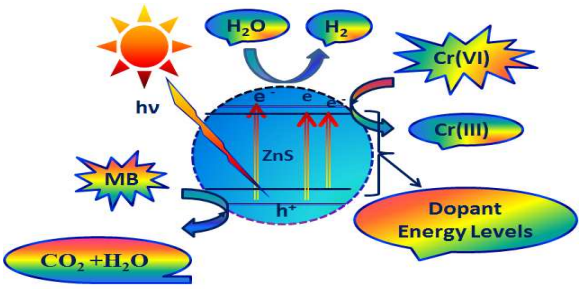

Journal Name

RSCPublishing

ARTICLE

Cite this: DOI: 10.1039/x0xx00000x
Received 00th January 2012,
Accepted 00th January 2012
DOI: 10.1039/x0xx00000x
www.rsc.org/

Novel synthesis of C, N doped rice grain shaped ZnS Nanomaterials –Towards enhanced visible light Photocatalytic activity for aqueous pollutant removal and H_2 production

A. Daya Mani[a], P. Ghosal[b] and Ch. Subrahmanyam[a*].

Novel single step syntheses of visible active C, N doped zinc sulfide (ZnS) photocatalysts with rice grain morphology has been achieved without using expensive surfactants, capping agents and inert atmospheric conditions by using solution combustion synthesis in an energy and time efficient manner. Several ZnS samples such as ZnS (1:2), ZnS (1:3), ZnS (1:4), ZnS (1:5) and ZnS (1:6) have been synthesized by varying metal and sulfur precursor ratio in order to obtain ZnS with desirable characteristics for visible light activity. X-ray diffraction indicated the nanocrystalline size and hexagonal ZnS phase, whereas, transmission electron microscopy confirmed the nanocrystalline size and also revealed the rice grain morphology for ZnS (1:5). Diffuse reflectance UV-Vis spectra indicated a red shift in the absorption maxima, possibly due to the decreasing band gap by C, N-doping, which was further confirmed by the elemental analysis and X-ray photoelectron spectroscopy. Visible light photocatalytic activity of the ZnS nanomaterials was assessed by high H_2 production (upto 10000 μmol/h/g for ZnS (1:5)) by water splitting in the presence of Na_2S and Na_2SO_3 sacrificial reagents, whereas, the simultaneous oxidation of MB and reduction of Cr(VI) under natural sunlight complemented the activity of ZnS.

1. Introduction

Depletion of the fossil fuel reserves and the increasing concentrations of greenhouse gases stimulated the research on the production of clean fuels [1]. Hydrogen, the cleanest fuel is expected to surpass the fossil fuels [2]. However, the conventional steam reforming of hydrocarbons for hydrogen production may no longer be environmental friendly due to the formation of carbon dioxide. Among the options available for hydrogen production, photocatalytic water splitting is attractive due to its environmentally benign nature [3-9]. However, despite the several reports on photocatalytic water splitting, there exists a need to develop robust catalysts. In a similar context, the conventional methods for the removal of aqueous pollutants are not so effective due to incomplete removal and/or generation of toxic byproducts [10,11]. Hence photocatalytic removal of these pollutants is gaining importance due to its ability for the mineralization of pollutants [12-16].

Although TiO_2 is proved to be the best photocatalyst under UV radiation, development of highly active photocatalysts that are active under the natural sunlight is still remains as a difficult task. There is a great demand for the synthesis of oxide and sulfide semiconductors that have high absorption in the visible radiation. Among them, ZnS is gaining interest owing to its favorable conduction band energy levels, and high theoretical efficiency of photo carrier generation than TiO_2 [17,18].

Even though ZnS nanomaterials with different morphologies have been reported by chemical or physical methods, these methods either use the expensive templates or the process is limited by low production yields [19-21]. In spite of the preferred negative reduction potential of zinc sulfide that favors hydrogen production, its high band gap becomes a thorn for its photocatalytic activity under solar light. Several studies have been carried out to increase visible light activity of ZnS by doping with metal ions and nonmetals [22, 23].

Combustion synthesis, a known method for the synthesis of oxide materials is gaining interest due to several advantages like shorter reaction times, non-expensive precursors, high surface area materials and in-situ anion doping [24-28]. In the present study, C and N doped zinc sulfide nanomaterials has been reported that do not demand the use of surfactants and capping agents. The visible light activity is assessed by the individual as well as simultaneous removal of Cr (VI) and methylene blue (MB) from aqueous solutions under natural sunlight. Also, H_2 production from water containing Na_2S and Na_2SO_3 sacrificial reagents was studied under simulated solar light.

2. Experimental section

Zinc nitrate and thiourea, the precursors of Zn and S were procured from Merck India was used as received. Sodium sulfide (Merck) and sodium sulphite (Merck) were used as sacrificial reagents for water splitting reaction. Milli Q-Plus water (resistance 18.2 MΩ) was used for all the experimental needs.

2.1. Synthesis of C, N doped ZnS nanomaterials

The instant synthesis of zinc sulfide is as follows: Different ratios (1:2 to 1:6) of zinc and sulfur precursors were used to prepare ZnS sulfide nanomaterials. In a typical synthesis aqueous solutions of zinc nitrate (oxidant) and thio urea (fuel) were mixed in

a quartz bowl and preheated on a hot plate until a viscous mass has been obtained, which was then transferred to a preheated furnace at 350° C. In 5 min a yellow colored material was obtained that is ready to be used for further photocatalytic studies. The samples were labeled as ZnS(1:2), ZnS(1:3), ZnS(1:4), ZnS(1:5) and ZnS(1:6). Since all the byproducts in this synthesis are gaseous products, immediately after combustion synthesis the samples can be used for the photocatalytic studies without the need of any post treatments like washing, calcination etc.

2.2. Characterization

Powder X-ray diffraction (PXRD) patterns of the as prepared zinc sulfide nanomaterials were recorded on PANalytical X'pert Pro powder X-ray diffractometer with Cu-Kα (1.5418 Å) radiation. The average crystallite sizes of the ZnS photocatalysts were calculated with the Scherrer equation with the full width at half maxima (FWHM) data. High resolution transmission electron microscopy (HRTEM) images of the combustion synthesized zinc sulfide photocatalysts were recorded using the TEM instrument operating at 200 kV using samples on copper grid (TECNAI G-2 with EDS model). UV-Vis diffuse reflectance spectra of the samples were measured by using Shimadzu UV-Vis spectrophotometer (UV-3600) between 200 and 800 nm range with $BaSO_4$ as a reference. The thermo gravimetric analyses of the as synthesized catalysts were recorded on TG/DTA, TA Instruments SDT Q600 in air flow from room temperature to 900° C with a heating rate of 10° C min-1. Percentage of C and N doped into the ZnS matrix was determined by using Euro EA elemental analyzer with sulfamethazine as a standard material which consists of 51.8 % C, 5.1 % H, 20.1 % N and 11.5 % S. X-ray Photoelectron Spectroscopic analysis of the samples were performed on Axis Ultra instrument under ultra-high vacuum condition (<10-8 Torr) and by using a monochromatic Al Kα X-ray source (1486.6 eV).

Photocatalytic activity of the rice grain shaped zinc sulfide nano structures has also been investigated by the individual and simultaneous removal of MB and Cr(VI) pollutants under the sunlight between 11 am to 1 pm. Before the exposure to sunlight, test solutions with photocatalyst were placed in dark in order to achieve equilibrium conditions. During the light exposure, every 15 min small aliquots were collected, centrifuged at an rpm of 2000 and the catalysts particles were separated by filtering with milli Q membrane filters. Thereafter MB and Cr(VI) were estimated by using UV-Vis spectrophotometer. At regular intervals of time the degradation of dye was monitored by the absorbance at 664 nm by using UV-Vis absorption spectroscopy. Cr (VI) was estimated by forming a purple coloured complex with 1, 5- Diphenyl hydrazide solution in acidic media. The concentration of Cr (VI) was estimated from the absorbance at 540 nm by using UV-Vis spectrophotometer.

The visible light activity of the ZnS photocatalysts was also estimated by the H_2 production experiments from water containing 1 M Na_2S and 1 M Na_2SO_3 as sacrificial agents under simulated solar light. H_2 production experiments were carried out in a photo reactor which consists of three 250 W halogen lamps. The intensity of the light falling on the sample cells was found to be 850-900 W/m^2 as measured by using Newport optical power/energy meter (Model 842. PE). The reaction cell was a quartz round bottomed flask containing 100 ml water and 100 mg of catalyst. Before addition of ZnS catalyst, N_2 was bubbled for 15 min, followed by evacuation for 15 min to remove the dissolved gases. After addition of the catalyst, the solution was stirred in dark for 30 min in order to facilitate the adsorption of water molecules on the ZnS surface. Hydrogen produced in the reaction was analyzed by using a Shimadzu gas chromatography (GC-2014) with packed column by using N_2 as the carrier gas. Every hour a 500 µl hydrogen gas was collected in a gas tight syringe (Hamilton) and injected into the GC column. The experiments performed both in dark and without catalyst in presence of light did not produce any hydrogen.

3. Results and Discussion

3.1. Formation mechanism of C and N doped ZnS

The synthesis of ZnS may proceed via the formation and decomposition of the zinc thiourea complex (Zn-$(SC(NH_2)_2)_2(NO_3)_2$). Therefore, in a typical tetrahedral or distorted tetrahedral Zn thiourea complex, $SC(NH_2)_2$ is coordinated to zinc through the sulfur atom, forming ZnS_4 groups [29]. As the nitrate is a monodentate ligand, it may be coordinated to zinc through the oxygen atom. Since the first coordination sphere of zinc complex contains, along with thiourea, the NO^{3-} anion, under the experimental conditions, thermal decomposition of Zn(SC-$(NH_2)_2)(NO_3)_2$ complexes results in the formation of C and N doped ZnS nanomaterials through the following reactions [30,31]. From the following reactions it is clear that with increasing ratio of sulfur presursor, the evolved gases also increases that also increses the amount of C and N doping in the ZnS matrix. This is consistent with the elemental analysis data.

$1\ Zn(NO_3)_2 + 2\ (NH_2)_2CS \longrightarrow ZnS + 2.2\ N_2 + 0.9\ CO_2 + 1.1\ HCNS + 3.4\ H_2O$ ------ (1)

$1\ Zn(NO_3)_2 + 3\ (NH2)_2CS \longrightarrow ZnS + 3.4\ N_2 + 1.3CO_2 + 1.7\ HCNS + 5.2\ H_2O$ ------ (2)

$1\ Zn(NO_3)_2 + 4\ (NH_2)_2CS \longrightarrow ZnS + 4.5\ N_2 + 1.7CO_2 + 2.3\ HCNS + 6.9\ H_2O$ ------ (3)

$1\ Zn(NO_3)_2 + 5\ (NH_2)_2CS \longrightarrow ZnS + 5.6\ N_2 + 2.1CO_2 + 2.8\ HCNS + 8.6\ H_2O$ ------ (4)

$1\ Zn(NO_3)_2 + 6\ (NH_2)_2CS \longrightarrow ZnS + 6.7\ N_2 + 2.6\ CO_2 + 3.4\ HCNS + 10.4\ H_2O$ ------ (5)

3.2. PXRD

Powder X-ray powder diffraction (PXRD) patterns of the ZnS samples as shown in **Fig.1** reveal the phase and crystallinity of ZnS nanostructures. The diffraction patterns of ZnS (1:2) to ZnS (1:6) can be indexed to the hexagonal ZnS (JCPDS card no 80-0007). From **Fig.1** it is observed that the diffraction peaks of (100) and (101) were overlapped with (002) diffraction peak due to peak broadening. The significant broadening of the diffraction peaks is ascribed to the very small crystallite size within the rice grain architecture. Moreover it is observed that the crystallinity of the samples also increased from ZnS (1:2) to ZnS (1:6).

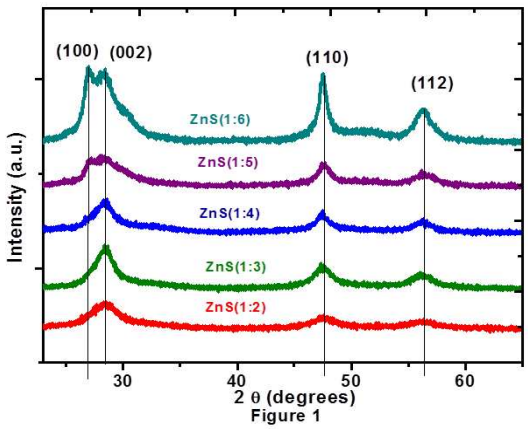

Fig.1. Powder X-Ray diffraction patterns of combustion synthesized zinc sulfide samples.

3.3. TEM

Fig. 2(a) shows a low magnification TEM image of the ZnS (1:5) sample. It clearly indicates that the sample is composed of well dispersed rice grain shaped microstructures which consist of

several nanoparticles of ZnS. The average size of the rice grain structure was around 1µm as estimated from the TEM image **Fig.2** (b) and magnified images (**Fig.2 (c) and (d))** confirm that the rice grain microstructures consist of several nanoparticles. The high magnification TEM image, as shown from **Fig.2 (c) to 2(d)** shows many nanoparticles with a clear contrast difference from each individual nanoparticle. This observation further confirms that the rice grain shaped microstructures consist of nanoparticles with a size of 10 nm which are assembled in a rice grain shaped structural configuration. Selected area electron diffraction (SAED) pattern of ZnS rice grain structures presented in the inset of figure 2(d) confirms (002), (110) and (112) planes characteristic of the hexagonal ZnS phase.

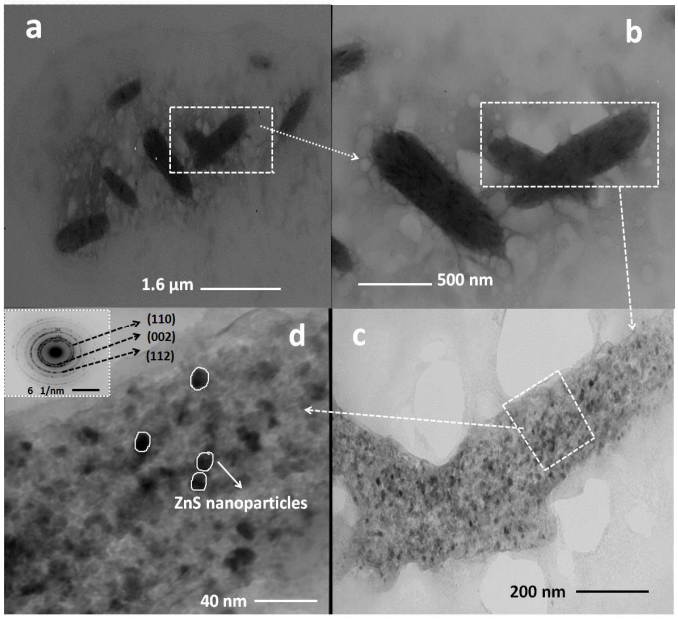

Figure 2

Fig.2. TEM image of ZnS rice grain microstructures (b) Enlarged view of the selected portion from **Fig.2(a)**. (c) Enlarged portion of rice grain shaped ZnS showing several nanoparticles (d) Further magnified view of the selected portion in **Fig.1 (c)** showing distinct nanoparticles of ZnS (inset shows selected area diffraction pattern of ZnS)

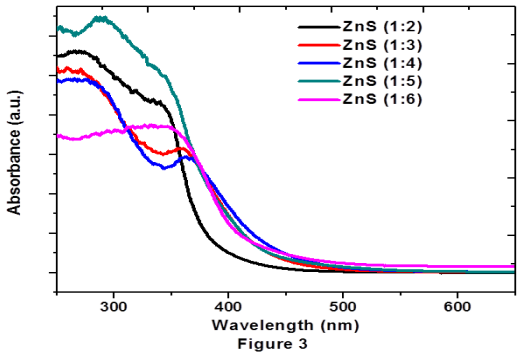

Figure 3

Fig.3. Diffused reflectance UV-Vis spectra of combustion synthesized ZnS samples

3.4. Diffuse reflectance UV-Vis spectral analyses

Diffuse reflectance UV-Vis spectra of the combustion synthesized ZnS samples are shown in **Fig.3**. A red shift in the absorption edge when compared to the conventional ZnS (3.7 eV) may be due to the in-situ C and N doping into ZnS during the combustion synthesis. The absorption onsets of all the combustion synthesized nano ZnS samples (430–460 nm) show significant red shifts (DE = 0.7–0.9 eV) with respect to that of bulk ZnS (onset- 350 nm) [32]. The onset edges for ZnS (1:2), ZnS (1:3), ZnS (1:4) ZnS (1:5) and ZnS (1:6) were calculated to be 3.0, 2.8, 2.8, 2.8 and 2.8 eV, respectively.

3.5. X-ray photoelectron spectroscopy

The composition and C, N doping in the ZnS matrix was further investigated by XPS. **Fig. 4** shows the XPS spectra of ZnS (1:5) sample. The ¬observed binding energies at 1045.0 and 1022.31 eV respectively corresponds to the Zn $2p_{1/2}$ and Zn $2p_{3/2}$ peaks (Fig. 4(a)) whereas S 2p spectra shown in **Fig. 4** (b) confirms a peak at 160.86 eV corresponding to the existence of sulfides [32].

XPS studies also revealed the presence of both C and N in ZnS nanomaterials. The deconvoluted N 1s (Fig. 4c) spectrum indicated two peaks which appeared at around 399.3 and 402.2eV that were attributed to Zn-N and/or C≡N bonds [33-36]. This is consistent with the literature observations, where the Zn-N bond of Zn_3N_2 and $ZnO_{1-x}N_x$ was observed at 396.2 and 399.1 eV, respectively. [35,36]. Therefore, we believe that the peak at 399.3 eV in **Fig. 4** (c) may be due to the Zn-N bond of ZnS_{1-x} N_x [20]. The slight chemical shift might be due to the surface strain and lattice distortion induced by the incorporation of nitrogen and carbon [37]. The peak appeared at 402.2 eV, may be attributed to an oxidized form of nitrogen or molecularly chemisorbed nitrogen (γ-N_2) [35,38].

Figure 4(d) shows the C 1s spectra of ZnS (1:5) catalyst. The peaks observed at 286.0 and 287.5 eV in **Fig. 4 (d)** can be attributed to C-N and C≡N bonds, respectively. The absence of peaks between 289.4 and 292.5 eV revealed the absence of C-O and O═C-O bonds, which is consistent with XRD observations that ZnS is free of ZnO impurity [34, 39]. The peak at 284.5 eV may be attributed to the elemental carbon (C-C) bond [40].

From the XPS studies it is concluded that the doping of carbon and nitrogen may be interstitial doping since the concentrations of dopants are relatively higher in the catalysts as observed from the CHNS analysis. Therefore XPS results and the higher N:C ratio observed in the elemental analysis suggests the possibility of Zn-N-C-N type linkage. Both the Zn and S atoms in the wurtzite structure are four coordinated and the structure is

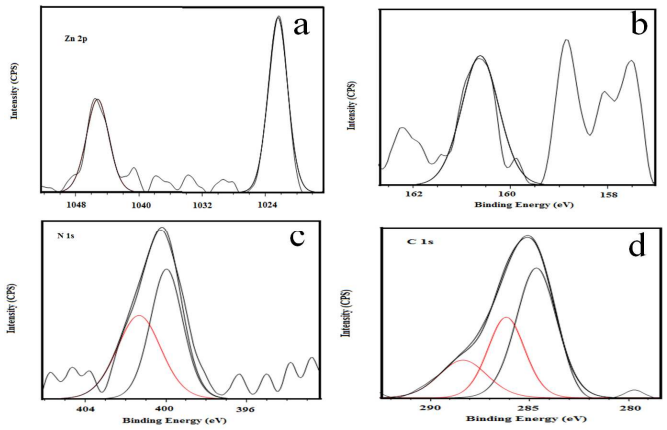

Figure 4

Fig.4. XPS spectra of (a) Zn 2p (b) S 2p (c) N 1s and (d) C 1s core levels.

composed of alternating planes of four coordinated S^{2-} and Zn^{2+} ions [41]. Therefore we speculate that the N-C-N linkage could bond with zinc and/or sulfur atom in the same plane or two adjacent planes and

could also exist in the interface of the planes, which may open a door for the possibility that N and C induce a higher energy band contributed by the localized N 2p and C 2p states. The amount of nitrogen and carbon is relatively higher in the synthesized catalysts, which reflects in the red shift in the band gap of ZnS from 3.6 to 2.8 eV.

3.6. CHNS Elemental Analyses

In order to analyze the weight percentage of C and N present in the combustion synthesized ZnS photocatalysts CHNS elemental analysis was carried out. The % C was found to be 6.8, 9.2, 13.1, 16.2, and 18.3 respectively for ZnS (1:2), ZnS (1:3), ZnS (1:4), ZnS (1:5) and ZnS (1:6) and the corresponding % of N was 10.4, 14.7, 22.8, 27.7 and 29.1. Thus the C and N doping in all the photocatalysts was also evidenced by elemental analyses.

3.7. Photocatalytic activity

3.7.1. Photocatalytic oxidation of MB

Photocatalytic activity of ZnS was estimated for the oxidation of methylene blue and photocatalytic reduction of chromium (VI) and the results are compared with a commercial photocatalyst (Evonik P25 TiO_2). **Fig. 5(a)** shows the first order kinetic plots for the oxidation of methylene blue under natural sunlight and the first order rate constant calculated was found to be 0.0039, 0.013, 0.015, 0.02, 0.026 and 0.021 min^{-1} respectively for Evonik P-25 TiO_2, ZnS (1:1), ZnS (1:2), ZnS (1:3), ZnS (1:4), ZnS (1:5) and ZnS(1:6). From this, it can be concluded that from ZnS (1:2) to ZnS (1:5) the activity steadily increased and thereafter it decreased slightly for ZnS(1:6). It clearly shows that ZnS (1:5) has highest activity among the ZnS samples.

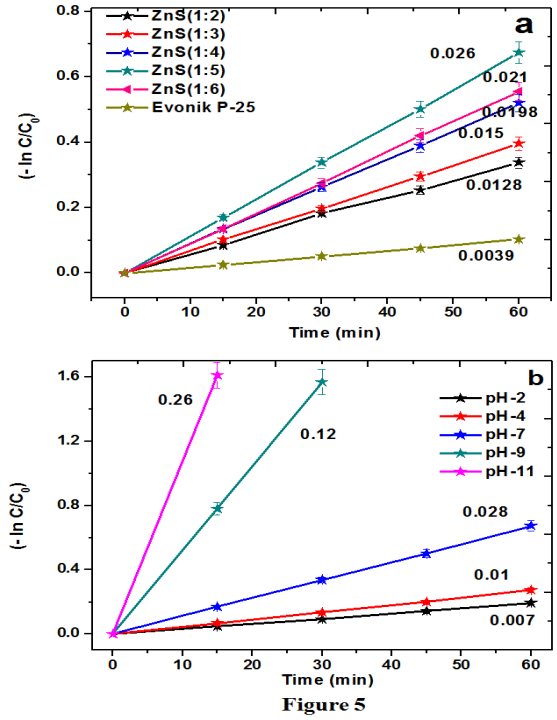

Figure 5

Fig.5. (a) First order reaction profiles of oxidation of MB by ZnS samples and commercial TiO_2 sample (C_0 (MB) = 20 ppm, catalytic amount=100 mg) (b) First order reaction profiles of oxidation of MB in the presence of different pH values (C_0 (MB) = 20 ppm, catalytic amount=100 mg, pH (2,4,7,9,11))

3.7.2. Effect of pH on photocatalytic oxidation of MB

It is well known that the pH of the medium can influence the rate of photocatalytic degradation of organic pollutants present in waste water. **Fig. 5(b)** shows first order kinetic plots for the effect of pH on the photocatalytic oxidation of MB. The first order rate constant values are found to be 0.25, 0.12, 0.026, 0.01 and 0.007 min^{-1} respectively at pH 11, 9, 7, 4 and 2. From this, it may be concluded that basic pH favors degradation of MB. This observation can be explained as follows: The pH of the solution affects the formation of hydroxyl radical, the primary oxidant during photocatalytic process. It is well known that at higher pH the concentration of OH^- ions will be more, which favors the formation of the $HO^\cdot$ radicals, thereby resulting in an increased photocatalytic degradation efficiency of MB [42]. On the other hand pH may also modify the electrical double layer of the solid electrolyte interface, which affects the adsorption-desorption processes and the separation of the photo generated electron-hole pairs in the surface of the catalyst particles [43]. In general the surfaces of photocatalysts are found to be positively charged in acidic solutions and negatively charged in alkaline solutions [44]. As a result, the efficiency of the MB photodegradation is expected to increase with pH owing to the electrostatic interactions between the negative photocatalyst surface and the MB cations. In addition to the above explanations higher pH also proved to be favourable for the oxidation of sulfur containing organic pollutants (MB) and decreases the deactivation of the catalyst [45].

3.7.3. Photocatalytic reduction of Cr(VI)

The activity of ZnS catalysts was also tested for the photocatalytic reduction of Cr(VI) under natural sunlight and the results are presented in Fig. 6a, which confirms first order kinetics. The corresponding first order rate constants were found to be 0.028, 0.036, 0.058, 0.1, 0.07 min^{-1} respectively for ZnS (1:2), ZnS (1:3), ZnS (1:4), ZnS (1:5) and ZnS(1:6). Thus during the reduction process also ZnS (1:5) shows higher activity.

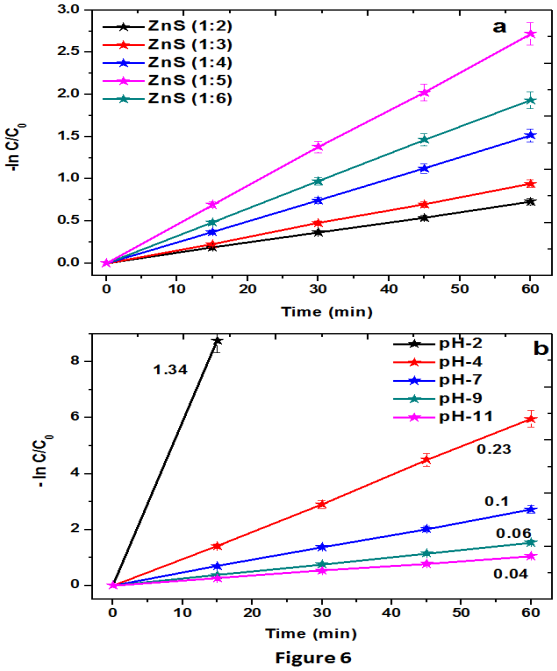

Figure 6

Fig.6. (a) First order reaction profiles of reduction of Cr(VI) by ZnS samples (C_0 (Cr(VI)) = 10 ppm, catalytic amount=100 mg) (b) Effect of pH on photocatalytic reduction of Cr(VI) (C_0 (Cr(VI)) = 10 ppm, catalytic amount=100 mg, pH (2,4,7,9,11)).

3.7.4. Effect of pH on photocatalytic reduction of Cr(VI)

Fig. 6 (b) shows the effect of pH (2-11) on the photocatalytic reduction of Cr (VI). As seen in the Fig. 6 (b), the photo reduction of Cr (VI) was 100 % within 15 min under acidic conditions (pH< 2). As shown in Fig. 6 (b), the rate constant was found to be 1.34, 0.23, 0.1, 0.06 and 0.04 min^{-1} respectively at pH of 2, 4, 7, 9 and 11. As reported by Chen and Cao [46], increasing pH decreases the adsorption capacity of the catalyst for dichromate ions. In general, Cr (VI) occurs in the forms of oxy anions like $HCrO_4^-$, $Cr_2O_7^{2-}$,CrO_4^{2-}, CrO_3, etc. The predominant form of Cr(VI) was the acid chromate species ($HCrO_4^-$) at lower pH that on increasing the pH, changes to other forms like CrO_4^{2-} and $Cr_2O_7^{2-}$ [46, 47]. Therefore, the ionic forms of Cr (VI) in solution and the charge of ZnS surface depend on the pH of the solution. Under the acidic conditions, the surface of the catalyst may be predominantly protonated and attracts the negatively charged Cr (VI) ions. In addition, under basic conditions, $Cr(OH)_3$ may be precipitated and cover the surface of the catalyst and decreases the activity of the catalyst.

3.7.5. Simultaneous oxidation of MB and reduction of Cr (VI)

Generally industrial waste waters consist of mixture of pollutants and simultaneous removal of these pollutants is beneficial. In addition, simultaneous treatment reduces the cost of the water treatment. **Fig.7** shows the first order kinetic plots for the simultaneous oxidation and reduction of MB and Cr(VI), respectively. A 50 ppm of Cr(VI) aqueous solution and 100 ppm of MB were taken as the combination of pollutants. It is worth mentioning that there is no reaction in the dark or without catalyst. From the rate constants, it is concluded that in case of simultaneous reaction the rate constant was found to be almost doubled than the individual reactions, which can be due to the suppression of electron hole recombination. Therefore simultaneous redox reactions not only decreases the water treatment cost but also increases the efficiency of the reaction.

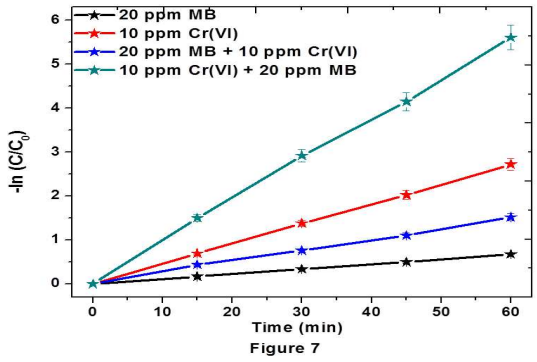

Figure 7

Fig.7. First order reaction profiles for the simultaneous removal of MB and Cr(VI) (C_0 (Cr(VI)) = 10 ppm, C_0 (MB) = 20 ppm catalytic amount=100 mg)

The best activity of ZnS (1:5) during photocatalytic activity may be explained as follows: With increasing sulfur precursor content from ZnS (1:2) to ZnS (1:5) there may be excess of free sulfide ions (due to insufficient zinc precursor), which can act like polysulfide ions and thereby can enhance both oxidation and reduction reactions on the surface of ZnS catalyst. But as observed in case of ZnS (1:6) the reduced activity might be due to the covering of active sites of ZnS by the far excess of sulfide residue. Thus the optimum ratio of oxidant and fuel might be achieved at 1:5. In addition to this M. Muruganandham et. al. have reported that C and N doping has a significant effect on the stability as well as photocatalytic properties of ZnS [50]. Therefore in our present study also C and N doping may have significant effect on the photocatalytic properties of the ZnS samples. CHNS elemental analysis confirmed the C and N doping that increased from ZnS(1:2) to ZnS (1:6). From this observation it may be concluded that the optimum C and N doping might be achieved for ZnS(1:5) sample and further increase of C and N doping may not be favorable for photocatalytic reactions.

3.7.6. Photocatalytic degradation mechanism of MB on C and N doped ZnS samples

The mechanism of pollutant degradation has been given in one of our publications [26]. Generally irradiation of a photocatalyst with energy suitable to that of band gap may promote a VB electron to the CB, leaving a hole in the VB (Eq. 6). Thereafter adsorbed water molecules on the photocatalyst surface react with these holes to form hydroxyl radicals, whose oxidation potential (2.8 V) is higher than many conventional oxidants like H_2O_2, ozone, etc [48]. On the other hand, in the conduction band the electron reduces the adsorbed oxygen to superoxide anion radical ($O_2^{\bullet-}$), which then reacts with water to form $^{\bullet}OH$ radical, as given in (Eqs. (10) and (11)). Consequently the reaction of $^{\bullet}OH$ radical with MB degrades the pollutant (Eq. (12)) [49].

$ZnS + h\nu \rightarrow h^+_{VB} + e^-_{CB}$ (6)

$h^+_{VB} + H_2O_{ads} \rightarrow H^+ + {}^{\bullet}OH$ (7)

$H_2O_{ads} \Leftrightarrow H^+_{ads} + OH^-_{ads}$ (8)

$h^+_{VB} + OH^-_{ads} \rightarrow {}^{\bullet}OH$ (9)

$e^-_{CB} + O_2 \rightarrow O_2^{\bullet-}$ (10)

$O_2^{\bullet-} + 2\,H_2O \rightarrow 2\,{}^{\bullet}OH + 2OH^- + O_2$ (11)

$^{\bullet}OH + MB \rightarrow$ degraded products (12)

3.7.7. Mechanism of photocatalytic reduction of Cr (VI)

The mechanism of Cr (VI) reduction may be explained as follows. The excitons produced upon irradiation of ZnS to suitable irradiation and the corresponding reactions of these excitons may be as follows as shown in Eq 13-15

Cr (VI) e-⟶ Cr (V) e-⟶⟶Cr (IV) e-⟶ Cr(III) (13)

$2H_2O + 4h^+ \rightarrow O_2 + 4H^+$ (14)

The overall reaction under acidic conditions (pH ≤ 2) may be summarized as follows:

$Cr_2O_7^{2-} + 14\,H^+ + 6\,e^- \rightarrow 2\,Cr^{3+} + 7\,H_2O$ (15)

3.7.8. Hydrogen production from water

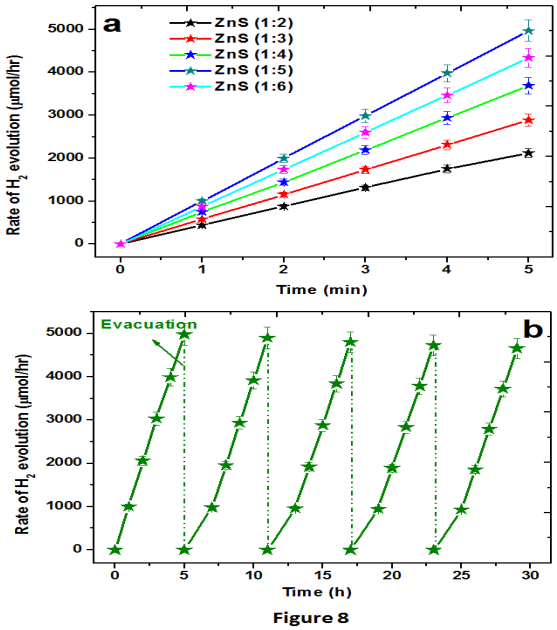

Figure 8

Fig.8. (a) Rate of H_2 evolution profiles from water containing 1M Na_2S and 1 M Na_2SO_3 sacrificial agents in the presence of all combustion synthesized ZnS samples for a period of 5 hr. (b) Rate of H_2 evolution profiles from water containing 1M Na_2S and 1 M Na_2SO_3 sacrificial agents in the presence of ZnS (1:5) (five runs in a continuous reaction were shown)

In order to further evaluate the visible light activity of ZnS photocatalysts H_2 production studies from water were performed. The studies were carried out in the presence of Na_2S and Na_2SO_3 as sacrificial reagents in order to prevent the photocorrosion of metal sulfide in presence of light. The studies were carried out continuously for 5 h without evacuation and the results are shown in **Fig. 8(a).** The observed rate of H_2 evolution was found to be 440, 580, 750, 999 and 870 μmol/h, respectively for ZnS(1:2), ZnS(1:3), ZnS(1:4), ZnS(1:5) and ZnS(1:6).

In order to study the stability of the photocatalyst under visible irradiation H_2 evolution studies were carried out for the most active ZnS(1:5) sample by studying five successive runs (25 h). The rate of H_2 evaluation with respect to time was given in **Fig. 8(b).** From **Fig. 8(b)** it is clearly observed that around 1000 μmol/h of H_2 was evolved and for every five hours of duration the reaction flask was evacuated to facilitate the empty space for the H_2 evolution. Five successive cycles of H_2 production were carried out and the decrease in H_2 production rate is found to be very less (approximately 7%) which indicates the good stability of the ZnS sample.

Conclusions

The important findings may be summarized as follows:
1) Novel one pot synthesis of visible active C, N doped ZnS nanomaterials with rice grain morphology without the need of costly precursors, surfactants and/or capping agents has been achieved under ambient conditions. A plausible formation mechanism has been proposed for the C and N doped ZnS nanomaterials.
2) ZnS nanomaterials showed excellent activity under visible radiation. A high activity for the H_2 production (upto 10000 μmol/h/g) was achieved from water containing Na_2S and Na_2SO_3 sacrificial agents under visible light.
3) It has been observed that simultaneous removal of Cr(VI) and methylene blue is more beneficial than mitigation of individual pollutants.
4) Studies on the effect of pH indicated that acidic conditions favor the reduction of Cr(VI), whereas, basic conditions favor MB oxidation.

Acknowledgements

Authors would like to thank Dr. Venugopal, IICT for the help. DM also would like to like to thank MHRD, India for UGC-JRF fellowship.

Notes and references

[a] Department of Chemistry, IIT Hyderabad, Yeddumailaram -502 205, India.
[b] Defence Metallurgical Research Laboratory, Kanchanbagh, Hyderabad 500 058, India.

1 A. J. Esswein and D. G. Nocera, *Chem. Rev*., 2007, **107**, 4022.
2 M. Z. Jacobson, W. G. Colella and D. M. Golden, *Science*., 2005, **308**, 1901.
3 X. Wang, K. Maeda, A. Thomas, K. Takanabe, G. Xin, J. M. Carlsson, K. Domen and M. Antonietti, *Nat. Mater*., 2009, **8**, 76.
4 K. Li, B. Chai, T. Peng, J. Mao and L. Zan, *RSC Adv*., 2013, **3**, 253.
5 J. Yu, Y. Yu and B. Cheng, *RSC Adv*., 2012, **2**, 11829.
6 J. Hou, C. Yang, Z. Wang, S. Jiao and H. Zhu, *RSC Adv*., 2012, **2**, 10330.
7 K. H. Reddy, S. Martha and K. M. Parida, *RSC Adv*., 2012, **2**, 9423.
8 R. Dom, R. Subasri, N. Y. Hebalkar, A. S. Chary and P. H. Borse, *RSC Adv*., 2012, **2**, 12782.
9 (a) L. Li, G. S. Rohrer and P. A. Salvador, *J. Am. Ceram. Soc.,* 2012, **95** 1414; (b) L. Li, P. A. Salvador and G. S. Rohrer, *Nanoscale*, 2014, **6**, 24.
10 G. Aragay, F. Pino and A. Merkoci, *Chem. Rev*., 2012, **112**, 5317.
11 K.-H. Kim and S.-K. Ihm, *J. Haz. Mater*., 2011, **186**, 16.
12 M. R. Hoffmann, S. T. Martin, W. Choi and D. W. Bahnemann, *Chem. Rev*., 1995, **95**, 69.
13 X. Liu, L. Pan, T. Lv, Z. Sun and C. Sun, *RSC Adv*., 2012, **2**, 3823.
14 H. Katsumata, Y. Oda, S. Kaneco and T. Suzuki, *RSC Adv*., 2013, **3**, 5028.
15 K.-J. Kim, P. B. Kreider, C. Choi, C.-H. Chang and H.-G. Ahn, *RSC Adv*., 2013, **3**, 12702.
16 V. Likodimos, D. D. Dionysiou and P. Falaras, *Rev. Environ. Sci. Biotechnol.,* 2010, **9**, 87.
17 J. S. Hu, L. L. Ren, Y.G. Guo, H. P. Liang, A.M. Cao, L. J. Wan and C. L. Bai, *Angew. Chem. Int. Ed.,* 2005, **44**, 1269.
18 S. L. Xiong, B. J. Xi, C. M. Wang, D. C. Xu, X. M. Feng, Z. C. Zhu and Y. T. Qian, *Adv. Funct. Mater*., 2007, **17**, 2728.
19 Y. Jiang, X.-M. Meng, J. Liu, Z.-Y. Xie, C.-S. Lee and S.-T. Lee, *Adv. Mater.,* 2003, **15**, 323.
20 H. Zhou, T. Fan, D. Zhang, Q. Guo and H. Ogawa, *Chem. Mater*., 2007, **19**, 2144.
21 Q. Zhao, L. Hou and R. Huang, Inorg. *Chem. Commun*., 2003, **6**, 971.
22 S. Biswas, S. Kar and S. Chaudhuri, *J. Phys. Chem. B*., 2005, **109**, 17526.
23 M. Muruganandham and Y. Kusumoto, *J. Phys. Chem. C.,* 2009, **113**, 16144.
24 K. Rajeshwar and N.R.D. Tacconi, *Chem. Soc. Rev*., 2009, **38**, 1984.
25 M.S. Hegde, G. Madras and K.C. Patil, *Acc. Chem. Res*., 2009, **42**, 704.
26 S. S. M. Bhat and N. G. Sundaram, *RSC Adv.,* 2013, **3**, 14371.
27 A. D. Mani, V. Laporte, P. Ghosal and Ch. Subrahmanyam, *Mater. Res. Bull.* 2012,**47**, 2415.
28 A. D. Mani, B. R. Raju, N. Xanthopoulos, P. Ghosal, B. Sreedhar and Ch. Subrahmanyam, *Chem. Eng. J.,* 2013, **228**, 545.
29 A.V. Naumov, V. N. Semenov and E. G. Goncharov, *Inorg. Mater.,* 2001, **37**, 539.
30 V. N. Semenov and A.V. Naumov, *Russ. J. Gen. Chem.,* 2001, **71**, 495.
31 A. A. Uritskaya, G. A. Kitaev and N. S. Belova, *Russ. J. Appl. Chem.,* 2002, **75**, 846.
32 K. Suzuki, K. Ikari and H. Imai, *J. Am. Chem. Soc.*, 2004, **126**, 462.
33 K. Sooklal, B. S. Cullum, S. M. Angel and C. J. Murphy, *J. Phys.Chem.,* 1996, **100**, 4551.
34 G. L. Chen, Y. Li, J. Lin, C. H. Huan, Y. P. Guo, *J. Phys. D:Appl. Phys.,* 1999, **32**, 195.

35 Y. H. Cheng, B. K. Tay, S. P. Lau, X. Shi, H. C. Chua, X. L. Qiao, J. G. Chen, Y. P. Wu and C. S. Xie, *Diamond Relat. Mater.*, 2000, **9**, 2010.
36 N. Tabet, M. Faiz and A. Al-Oteibi, *J. Electron Spectroc. Relat.Phenom.,* 2008, **163**, 15.
37 M. Mapa and C. S. Gopinath, *Chem. Mater*., 2009, **21**, 351.
38 J. Yang, H. Bai, X. Tan and J. Lian, *Appl. Surf. Sci.,* 2006, **253**, 1988.
39 L.-C.Chen, Y.-J. Tu, Y.-S. Wang, R.-S. Kan and C.-M. Huang, *J. Photochem. Photobiol. A* 2008, **199**, 170.
40 Y.-H. Tseng, C.-S. Kuo, C.-H. Huang, Y.-H. Li, P.-W. Chou, C.-L. Cheng and M.-S. Wong, *Nanotechnology*, 2006, **17**, 2490.
41 H. Pan, J. B. Yi, L. Shen, R. Q. Wu, J. H. Yang, J. Y. Lin, Y. P. Feng, J. Ding, L. H. Van and J. H. Yin, *Phys. Rev. Lett.*, 2007, **99**, 127201.
42 D. Moore and Z. L. Wang, *J. Mater. Chem.,* 2006, **16**, 3898.
43 K.M. Parida, N. Sahu, N.R. Biswal, B. Naik and A.C. Pradhan, *J. Colloid. Interface Sci.,* 2008, **318**, 231.
44 A. Franco, M.C. Neves, M.M.L.R. Carrott, M.H. Mendonça, M.I. Pereira and O.C. Monteiro, *J. Hazard. Mater.,* 2009, **161**, 545.
45 W.Z. Tang and C.P. Huang, *Chemosphere*, 1995, **30**, 1385.
46 A.P. Davis and C.P. Huang, *Water Res.,* 1991, **25**, 1273.
47 S. F. Chen and G.Y. Cao, *Chemosphere.*, 2005, **60**, 1308.
48 N. Tewari, P. Vasudevan and B.K. Guha, *Biochem. Eng. J.*, 2005, **23**, 185.
49 P.R. Gogate and A.B. Pandit, *Adv. Environ. Res.*, 2004, **8**, 501.
50 M. Muruganandham, A. Ramakrishnan, Y. Kusumoto and M. Sillanpaa, *Phys. Chem. Chem. Phys*., 2010, **12**, 14677.